Lipofuscin causes atypical necroptosis through lysosomal membrane permeabilization

Chendong Pan[a,1], Kalpita Banerjee[a,1], Guillermo L. Lehmann[a], Dena Almeida[b], Katherine A. Hajjar[b], Ignacio Benedicto[a,c], Zhichun Jiang[d], Roxana A. Radu[d], David H. Thompson[e], Enrique Rodriguez-Boulan[a], and Marcelo M. Nociari[a,2]

[a]Department of Ophthalmology, Weill Cornell Medicine, Margaret Dyson Vision Research Institute, New York, NY 10065; [b]Department of Pediatrics, Weill Cornell Medicine, New York, NY 10065; [c]Centro Nacional de Investigaciones Cardiovasculares, Madrid 47907, Spain; [d]UCLA Stein Eye Institute, Department of Ophthalmology, University of California, Los Angeles, CA 90095; and [e]Department of Chemistry, Purdue University, West Lafayette, IN 28029

Edited by Anand Swaroop, National Eye Institute Neurobiology Neurodegeneration and Repair Laboratory, Bethesda, MD, and accepted by the Editorial Board September 22, 2021 (received for review January 19, 2021)

Lipofuscin granules enclose mixtures of cross-linked proteins and lipids in proportions that depend on the tissue analyzed. Retinal lipofuscin is unique in that it contains mostly lipids with very little proteins. However, retinal lipofuscin also presents biological and physicochemical characteristics indistinguishable from conventional granules, including indigestibility, tendency to cause lysosome swelling that results in rupture or defective functions, and ability to trigger NLRP3 inflammation, a symptom of low-level disruption of lysosomes. In addition, like conventional lipofuscins, it appears as an autofluorescent pigment, considered toxic waste, and a biomarker of aging. Ocular lipofuscin accumulates in the retinal pigment epithelium (RPE), whereby it interferes with the support of the neuroretina. RPE cell death is the primary cause of blindness in the most prevalent incurable genetic and age-related human disorders, Stargardt disease and age-related macular degeneration (AMD), respectively. Although retinal lipofuscin is directly linked to the cell death of the RPE in Stargardt, the extent to which it contributes to AMD is a matter of debate. Nonetheless, the number of AMD clinical trials that target lipofuscin formation speaks for the potential relevance for AMD as well. Here, we show that retinal lipofuscin triggers an atypical necroptotic cascade, amenable to pharmacological intervention. This pathway is distinct from canonic necroptosis and is instead dependent on the destabilization of lysosomes. We also provide evidence that necroptosis is activated in aged human retinas with AMD. Overall, this cytotoxicity mechanism may offer therapeutic targets and markers for genetic and age-related diseases associated with lipofuscin buildups.

Lipofuscin | necroptosis | LMP | lipid-bisretinoids | aging

Lipofuscin is an indigestible mixture of fluorescent cross-linked proteins and lipids that accumulates in the lysosomes of many nondividing cells. Its composition varies with the tissue analyzed. Retinal lipofuscin differs from other lipofuscins in that it is mostly lipid-bisretinoids with almost no proteins (1). However, retinal lipofuscin also presents a number of characteristics that make it indistinguishable from conventional lipofuscin granules. Specifically, 1) it is an indigestible material that fills irreversibly the lumen of lysosomes and affect their degradative, sensing and signaling functions (2); 2) it causes lysosomal swelling, linked to increased susceptibility to rupture (3–5); 3) it triggers NLRP3 (NOD-, LRR-, and pyrin domain-containing protein 3) inflammation, indicative of low-level lysosomal disruption (6, 7); 4) retinal lipofuscin is also an autofluorescent pigment that serves as biomarker of aging (8, 9); and 5) it is considered toxic waste (10, 11).

Retinal lipofuscin accumulates in the retinal pigment epithelium (RPE), a single layer of epithelial cells that separates the neuroretina from the choroidal blood vessels. RPE cells are long lived, do not divide, and each cell is responsible for the phagocytic removal of massive amounts of waste, daily produced by its numerous overlying photoreceptors (12, 13). This incessant and endless clearance demand predisposes the RPE to experience buildups of lipofuscin with time. The lipid-bisretinoids found in retinal lipofuscin are a family of at least 27 structurally related autofluorescent lipo-pigments, among which N-retinilidene-N- retinyl ethanolamine (A2E) and all-trans-retinal dimer (ATRD) are the most abundant ones (1, 14). Lipid-bisretinoids are slowly generated in photoreceptors by the spontaneous dimerization of vitamin A aldehydes involved in the synthesis of visual pigments (15, 16). This dimerization is dramatically accelerated by mutations in the Abca4 gene that encodes a flippase that transfers retinaldehydes from photoreceptor discs to the cytosol, in which retinal dehydrogenases (RDH8 in mice) reduce them to retinols. Photoreceptor bisretinoids are transferred by phagocytosis into RPE lysosomes in which, due to their resistance to hydrolysis, accumulate permanently in lipofuscin granules (5). Their progressive accumulation with age or their fast accumulation through genetic mutations in Abca4 may lead to primary RPE cell death and secondary death of photoreceptors, a phenotype found respectively in atrophic Age-related Macular Degeneration (dry AMD) and Stargardt disease (17–19).

Significance

Retinal lipofuscin causes retinal pigment epithelium cell death in Stargardt and potentially dry–Age-Related Macular Degeneration (AMD). The current dogma is that lipofuscin's cytotoxicity results from the light-triggered decomposition of its lipid-bisretinoids leading to apoptosis. However, antiapoptotic antioxidants or light-blocking lenses are not effective to stop degeneration in Stargardt and most AMD patients. Here, we show that lipofuscin forms aggregates in lysosomes, which trigger lysosomal membrane permeabilization and subsequent atypical necroptosis. We provide evidence that necrosulfonamide, necrostatin-7, and arimoclomol can effectively control this lethal cascade.

Author contributions: C.P., K.B., and M.M.N. designed research; C.P., K.B., G.L.L., I.B., Z.J., R.A.R., and M.M.N. performed research; G.L.L., D.A., K.A.H., D.H.T., and E.R.-B. contributed new reagents/analytic tools; C.P., K.B., E.R.-B., and M.M.N. analyzed data; and C.P., K.B., E.R.-B., and M.M.N. wrote the paper.

Competing interest statement: A patent has been filed for targeting the LMP/necroptosis cascade.

This article is a PNAS Direct Submission. A.S. is a guest editor invited by the Editorial Board.

[1]C.P. and K.B. contributed equally to this work.

[2]To whom correspondence may be addressed. mnociari@med.cornell.edu.

This article contains supporting information online at http://www.pnas.org/lookup/suppl/doi:10.1073/pnas.2100122118/-/DCSupplemental.

Published November 15, 2021.

Currently, the underlying mechanisms of retinal lipofuscin cytotoxicity are incompletely understood, and the strategies to modulate them are not effective. The dominant dogma is that RPE cell death is caused by the phototoxic decomposition of lipid-bisretinoids, leading to oxidative stress and apoptosis (20–22). However, retinal damage by ambient light was only evident in albino mice (23), and there is no evidence that antioxidants, light blockage, or anti-apoptotic drugs provide any benefit against degeneration in pigmented retinas overloaded with lipofuscin (24, 25) in which photodegradation of lipid-bisretinoids is considerably diminished (23). All these suggest the existence of light-independent cell-death mechanisms that need to be deactivated in order to protect against lipofuscin.

Here, we demonstrate that lipofuscin promotes retinal degeneration via a light-independent atypical necroptotic cascade. The pathway that we describe is fundamentally different from previously reported mechanisms of RPE cell death, as it does not involve oxidative stress, apoptosis, or classical necrosomes containing Receptor-interacting serine/threonine-protein kinase 1 (RIPK1) or Receptor-interacting serine/threonine-protein kinase 3 (RIPK3) kinases (26) and implicates lysosomal membrane permeabilization (LMP). Importantly, light-independent lipofuscin-elicited necroptosis was prevented with necrosulfonamide (NSA), necrostatin-7 (Nec7), and arimoclomol, a drug that preserves lysosomal integrity. Summarizing, the present work provides directions to develop potential treatments for Stargardt disease that could eventually be applied to treat other pathological conditions associated with accumulation of lipofuscins.

Results

Association between Lipofuscin Buildup and Retinal Degeneration. We carried out experiments in the eyes of Abca4$^{-/-}$Rdh8$^{-/-}$ (DKO) mice, because they exhibit the highest and fastest buildup of lipofuscin in their RPE layer, as a result of the double mutation (27). Using confocal microscopy on flat-mounted eyecups peeled off their neuroretinas to measure the RPE lipofuscin fluorescence, we noticed that 8-mo DKO animals exhibited three times more fluorescence than age-matched wild-type (WT) controls (Fig. 1*A*, flat mounts). Furthermore, lipofuscin levels in DKO 25 mo-old were three times higher than in WT 33 mo-old (Fig. 1*A*, flat mounts). Higher-magnification imaging revealed that the increase was caused by a rise in the number of lipofuscin granules per RPE cell (Fig. 1*A*, small inserts). Using phalloidin staining to delineate cell borders, we noticed that whereas in WT retinas, RPE cells maintained their typical uniform hexagonal geometry, in DKO retinas, RPE cells deteriorated progressively with age, so that by 24 mo, the RPE layer contained mostly scattered giant-multinucleated cells with intracellular stress fibers (Fig. 1*B*). We then quantified the lipofuscin levels per cell in RPE flat mounts of different age DKO mice and compared them with the levels in 33-mo-old WT. The lipofuscin per RPE increased uninterruptedly with age (Fig. 1*C*), which was confirmed in cross-sectional images of DKO retinas (Fig. 1*D*). Additionally, this continuous age-related cumulative trend of lipofuscin in the RPE was confirmed by high-performance liquid chromatography (HPLC) (*SI Appendix*, Fig. S1).

To detect degenerative changes, we quantified the size (area in micrometers^2) of the central retina's RPE cells in 8- and 23-mo-old flat mounts devoid of neuroretina (Fig. 2*A*). The average area of RPE cells changed from around 411.4 ± 10.9 μm^2 to 506.2 ± 15.9 μm^2 (range from 134 to 1,873 μm^2) in WT retinas compared to 434.1 ± 14.4 μm^2 to 1,018 ± 77.9 μm^2 (range from 143 to 4,896 μm^2) in DKO retinas. This enlargement of RPE cells in DKO retinas correlated with a significant decrease in the number of RPE nuclei compared to age-matched WT retinas ($P < 0.05$) (Fig. 2*B*) and significantly fewer photoreceptors, from center to periphery, in 26-mo-old DKO compared to same-age WT mice (Fig. 2*C*). Moreover, confocal microscopy of cryo-sections obtained from old DKO (8 to 30 mo-old) retinas revealed the presence of small (~1 to 3 μm) lipofuscin debris in the neuroretina, which were absent in WT controls (Fig. 2*D*). These specks stained positive for Iba1, rhodopsin (Fig. 2*E* and *SI Appendix*, Fig. S8), and CD11b (*SI*

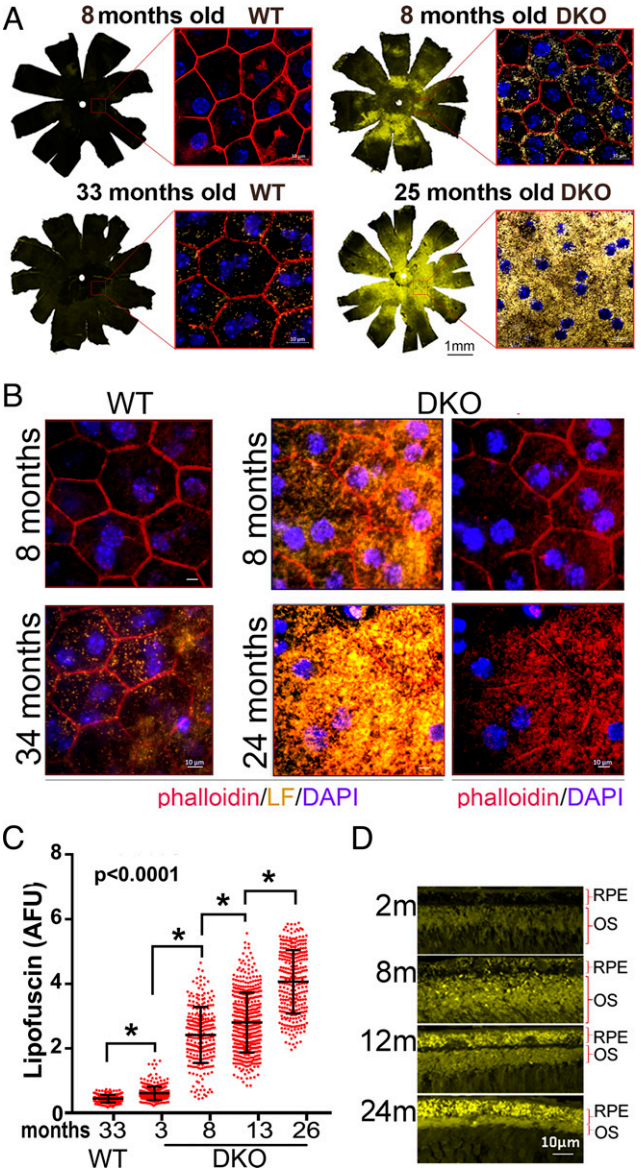

Fig. 1. (*A*) Llipofuscin content in RPE of WT and DKO mice at indicated ages. Fluorescence images of RPE flat mounts (10×) were stitched together to display the content in the whole eye. The orientation is as follows: dorsal–top; nasal–right. (Scale bar, 1 mm.) Inserts show high-magnification (63×) of central-retina RPE, with lipofuscin granules (yellow), ZO1 borders (red), and a nuclear Hoechst (blue). (Scale bars, 10 μm.) (*B*) 63× image of central retina's RPE. Phalloidin are in red and lipofuscin granules are in yellow. Hexagonal RPE shape in both 8- and 34-mo WTs (*Left* two panels) contrasts with giant cells with lipofuscin in 8 and 24 mo DKOs. (Scale bars, 10 μm.) (*C*) Lipofuscin content per RPE, calculated from random fluorescent fields in flat-mounted RPE eyecups prestained with phalloidin. A 33-mo-old WT ($n = 5$) exhibited less lipofuscin/cell than 3-mo-old DKO ($n = 4$) ($P < 0.01$). The content of lipofuscin/cell was significantly different between 3- and 8- ($n = 6$); 8- and 13- ($n = 4$); and 13- and 26 ($n = 5$)-mo-old DKOs (mean ± SD, $P < 0.0001$). (*D*) Paraffin cross-section showing the progressive accumulation of lipofuscin in the RPE of DKO mice with age.

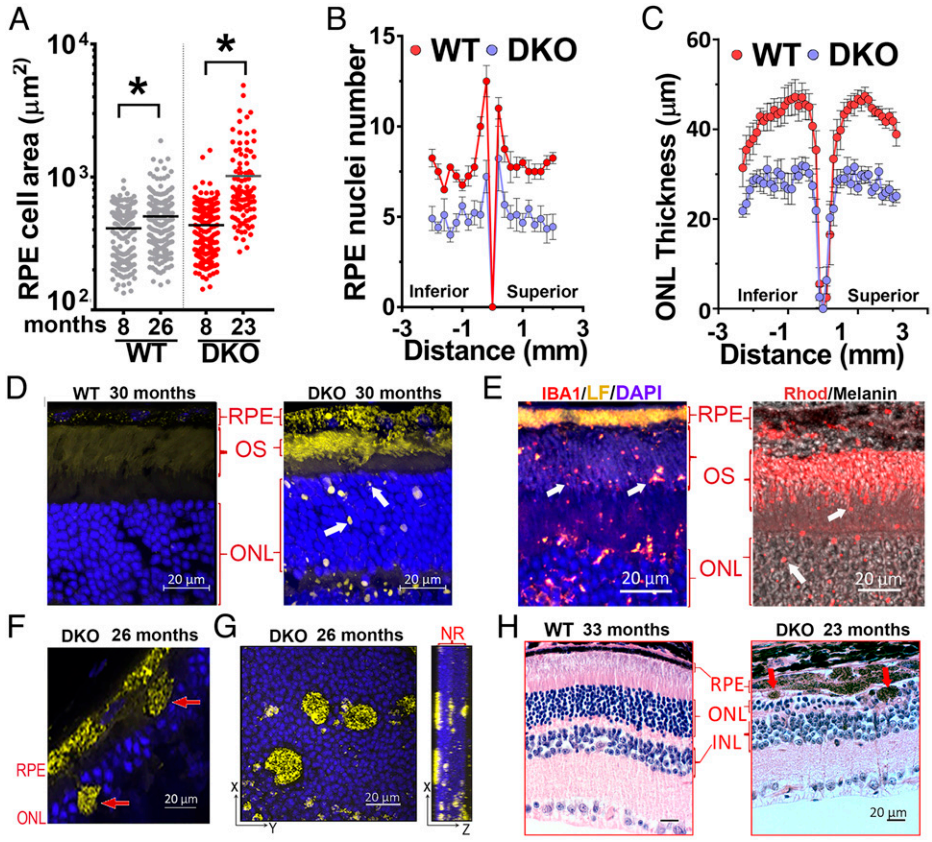

Fig. 2. Degeneration in retinas with lipofuscin. (*A*) Individual and mean values of RPE's sizes (micrometers^2) in flat mounts from 8 ($n = 5$)- and 26 ($n = 5$)-mo-old WT (gray); 8 ($n = 6$)- and 23 ($n = 5$)-mo-old DKO (red) ($P < 0.0001$, unpaired t test). (*B*) RPE nuclei number in 26-mo-old DKO (blue) ($n = 10$) and WT (red) ($n = 8$) measured in paraffin cross-sections every 0.2 mm ($P < 0.05$, mean ± SEM, by multiple t tests). (*C*) ONL thicknesses in hematoxylin and eosin (H&E) stained cross-sections, along the vertical axis, in 26-mo-old DKO (blue) ($n = 5$) and WT (red) ($n = 7$) ($P < 0.001$, mean ± SEM, by ordinary two-way ANOVA). (*D*) Autofluorescence (yellow) in cryo-sections from 30-mo-old WT ($n = 3$) and DKO ($n = 3$) showing ~1 to 3 μm lipofuscin debris (white arrows). (*E*, *Left*) ~1 to 3 μm lipofuscin debris colocalize with Iba1 (white arrows) in 20-mo-old DKO retina. (*E*, *Right*) ~1 to 3 μm lipofuscin debris (white arrows) are positive for rhodopsin (red) in 10-mo-old DKO. Bright-field image was overlapped to show RPE-melanin (black). (*F*) ~5 to 10 μm RPE debris (arrows) in paraffin-section of 26-mo-old DKO. (*G*) Maximum projection of z-stacks from 26-mo-old DKO flat-mounted neuroretina. Noticeable were the large RPE debris inserted at different depths into the ONL. (*H*) H&E cross-sections. (*Right*) Damage in ONL overlying ~10 μm RPE debris containing melanin. (Scale bars, 20 μm.)

Appendix, Fig. S2*A*), suggesting that they represent small pieces of photoreceptors engulfed by phagocytic cells (Fig. 2*A* and *SI Appendix*, Fig. S2*B*).

We also noticed much-larger lipofuscin debris (~5 to 10 μm) containing melanin, shed from the RPE layer (Fig. 2 *F* and *G*). Importantly, the outer nuclear layer (ONL) in close proximity to the areas of RPE shedding, appeared thin and disorganized (Fig. 2*H*), indicative that the photoreceptors were particularly affected by these RPE anomalies. TUNEL (terminal deoxynucleotidyl transferase dUTP nick end labeling) staining on frozen sections confirmed abundant dead photoreceptors in those areas (*SI Appendix*, Fig. S2*C*). Overall, these data indicate a direct correlation between accumulation of lipofuscin granules in the RPE and accelerated degeneration of the retina.

Lipofuscin Photooxidation and Retinal Degeneration. The contribution of photooxidation to the degenerative process remains uncertain for pigmented retinas. Since photooxidation of lipid-bisretinoids can be completely stopped, without affecting their formation, by rearing animals in darkness (23, 28), we asked whether RPE and photoreceptor health would be preserved in mice never exposed to light. Hence, we housed WT and DKO pigmented mice from birth in either continuous darkness or under 12-h cyclic-light conditions. We evaluated the thickness of their ONL as well as the number of RPE nuclei after 1 y. Strikingly, lipofuscin-associated thinning of the ONL and reduction of RPE number proceeded at similar rates independently of whether the mice were light cycled or dark reared (Fig. 3). Surprisingly, the loss of RPE cells, even in dark-reared DKOs, was concentrated in the inferior hemisphere (Fig. 3). In parallel, WT groups showed no significant loss of photoreceptors or RPE cells during the same period irrespective of illumination conditions. To verify that lipofuscin had still accumulated in the absence of light, we imaged the autofluorescence of RPE flat mounts devoid of neuroretina in 12-mo-old mice from each of the four groups (*SI Appendix*, Fig. S3). Indeed, dark-reared WT and DKO mice contained ~2.8 and approximately five times more lipofuscin than their counterparts reared under cyclic-light conditions, respectively ($P < 0.05$). These in vivo results demonstrate that the deterioration of RPE and photoreceptors in pigmented retinas loaded with lipofuscin is driven largely by light-independent cytotoxic cascades.

Mechanisms of Light-Independent Cell Death. In order to study light-independent, lipofuscin-mediated cell death, we adapted existing protocols for incorporating lipid-bisretinoids (A2E and ATRD) into the lysosomes of cultured RPE (ARPE-19) cells (29). Using this in vitro model, we observed a dose-dependent, light-independent cytotoxicity (Fig. 4*A*). The susceptibility to lipofuscin depended heavily on cell confluency (*SI Appendix*, Fig. S4*A*), as denser cultures were more impervious to incorporate lipid-bisretinoids (*SI Appendix*, Fig. S4*B*). *SI Appendix*, Fig. S4*C* shows that this effect was not due to the formation of

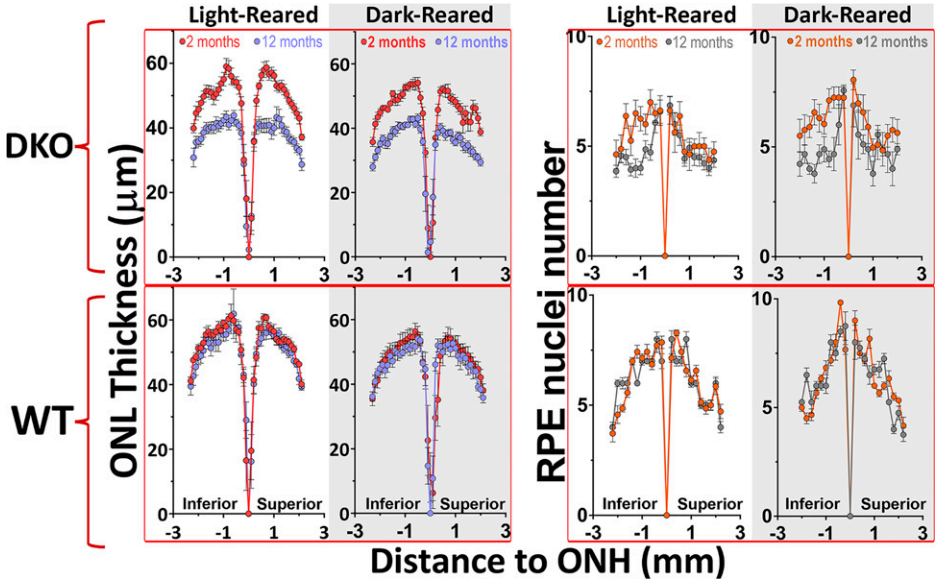

Fig. 3. Light-independent lipofuscin cytotoxicity contributes to degeneration in pigmented retinas. ONL thinning and nuclei RPE loss, between 2 and 12 mo of age, occurred at similar levels among light-cycled and dark-reared mice ($P < 0.01$, by two-way ANOVA). For ONL: 12 h-light-cycled mice, 2-mo DKO ($n = 8$); 12-mo DKO ($n = 14$); and 2- and 12-mo WT ($n = 6$ per group). For dark-reared: 2-mo DKO ($n = 6$); 12-mo DKO ($n = 8$); and 2- and 12-mo WT ($n = 6$ per group). For RPE nuclei number: 12 h-light-cycled mice, 2-mo DKO ($n = 8$); 12-mo DKO ($n = 14$); and 2- and 12-mo WT ($n = 7$ per group). For dark-reared: 2-mo DKO ($n = 7$); 12-mo DKO ($n = 4$); and 2-mo ($n = 4$) and 12-mo WT ($n = 7$) ($P < 0.05$, mean ± SEM, by multiple *t* test).

multilayers during the assay. The efficiency of the A2E incorporation was similar for different doses (*SI Appendix*, Fig. S4*D*). Hence, we chose 80% confluency for our assays, because under these conditions, ARPE-19 cells took up 80% of supplemented lipid-bisretinoids, reaching lipofuscin levels in the range of those found in the RPE of DKO mice (*SI Appendix*, Fig. S4*E*). Using this in vitro setup, we then confirmed that lipofuscin elicited light-independent cell death in differentiated human fetal RPE (hfRPE) cells (*SI Appendix*, Fig. S4*F*).

Next, we investigated whether the RPE cell death induced by lipofuscin was apoptosis or necrosis. For light-independent death, cells were incubated with 30 μM A2E or 80 μM ATRD from the beginning of the experiment. For light-dependent death, cells received sublethal doses (i.e., 10 μM A2E or 25 μM ATRD) 24 h before the beginning of the experiment, which started immediately after exposing cells 10 min to blue light. To this end, we added to the media NucView405 a nonfluorescent, cell-permeable substrate that stains nuclear DNA blue when cleaved by caspase 3 during the executioner phase of apoptosis and DRAQ7, a dye that stains nuclear DNA far-red only if cells have compromised membrane integrity. By monitoring the fluorescence at 30-min intervals, we established that lipofuscin in the absence of light induced early membrane compromise, consistent with necrosis, while if exposed to blue light, cells died from apoptosis (Fig. 4*B*). Interestingly, ATRD was a less-potent inducer of necrosis and apoptosis than A2E, although it carried the same aldehyde group touted as responsible for the high toxicity of its precursor all-transretinal (ATR) (30, 31).

It has been proposed that A2E could cause light-independent nonprogramed necrosis through its detergent behavior, because it contains a hydrophilic pyridinium head and two hydrophobic chains (32). To investigate this possibility, we fed cells with a soluble form of A2E (i.e., A2E complexed with methyl beta cyclodextrin) (MβCD-A2E). MβCD–guest complexes allow the efficiently pinocytic delivery of guest molecules into lysosomes (33) without permitting their plasma membrane intercalation (34). In parallel, we fed MβCD–Triton X-100 complexes (35) to confirm that under these conditions, MβCD could effectively neutralize amphipathic molecules' detergent activity. Remarkably, MβCD did not protect against A2E while it fully neutralized Triton's toxicity (Fig. 4*C*). This result plus the slow kinetics of cell death (several hours versus instantaneous death with Triton) suggested that A2E triggers a form of programmed necrosis.

To identify the type of necrotic program, we attempted protection of cells, challenged by lipofuscin, with inhibitors of the main known effector pathways of programmed cell death (36, 37). Thus, we used a pan-caspase inhibitor (z-VAD(OMe)-FMK) for apoptosis, disulfiram (38) for Gasdermin-D induced pyroptosis, the potent iron chelator, Deferoxamine (DFO), for ferroptosis (39), and NSA for Mixed Lineage Kinase domain-Like (MLKL)–induced necroptosis (26) (Fig. 4*D*). Only pretreatment with NSA, a drug that blocks the spontaneous assembly of phospho-MLKL into oligomeric pores that insert into membranes and kill the cell (40), increased survival in a dose-dependent manner. Considering that phosphorylation of MLKL, at Ser358 in humans (or the equivalent Ser345 in mouse) is a hallmark trigger event and a marker of necroptosis (41), we determined the Ser358 phosphorylation and polymerization status of MLKL in ARPE19 cells loaded with lipofuscin. Using Western blotting under nonreducing conditions to preserve and increase the chances of detecting phospho-oligomers, we demonstrated that A2E (Fig. 4*E*) as well as ATRD (Fig. 4*F*) cause dose-related phosphorylation and polymerization of MLKL in the absence of light. We then checked for protection with drugs that powerfully inhibit necrosomes (i.e., multiprotein complexes in which MLKL gets phosphorylated, mostly by RIPK3) (42). The necrosome complex changes depending on the stimulus triggering the necroptosis. It usually contains RIPK1 (43). Necrostatins 1, 1s, 2, and 5 are all selective inhibitors of RIPK1, while Nec7 targets an unknown regulatory molecule in the pathway (44). Surprisingly, RIPK1-targeting necrostatins provided no survival benefit, whereas Nec7 was very protective (Fig. 4*G*). More unpredicted was the observation that GSK′872, GSK′840, and GSK′843, all highly selective inhibitors of RIPK3 (the only known kinase to phosphorylate MLKL), did not protect either against cell death (Fig. 4*G*). Along the same direction, Western blot results showed that while treatment with Nec7 stopped lipofuscin-induced phosphorylation and polymerization of MLKL, treatment with Nec1 or GSK′872, did

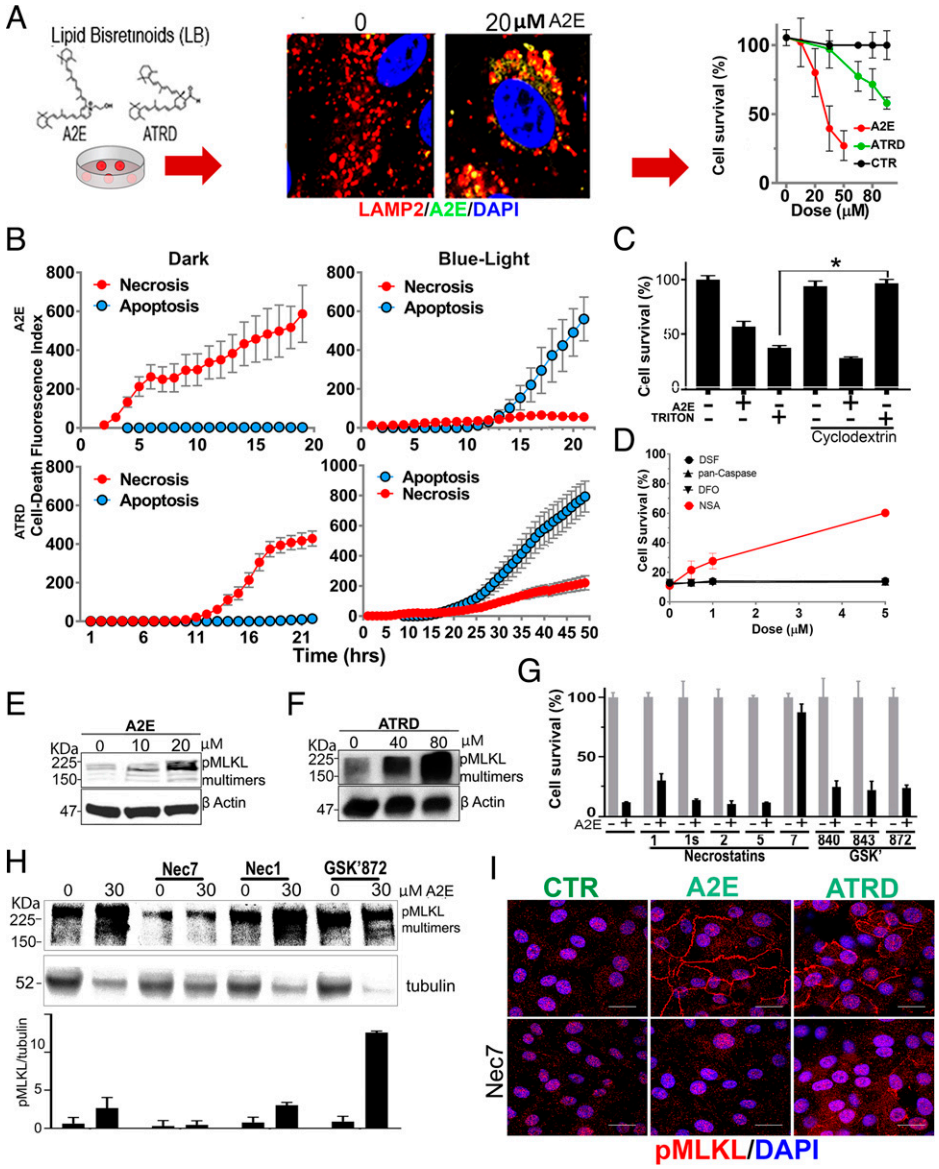

Fig. 4. Mechanism of light-independent cytotoxicity. (*A*) Lipid-bisretinoids accumulation (green) into lamp-2 lysosomes (red) of ARPE-19 in cell-death assay. Viability was determined with Resazurin. (*B*) Real-time monitoring of apoptotic and necrotic death in ARPE19 cells in the dark or after blue-light exposure. For dark toxicity, cells received A2E (30 μM) or ATRD (80 μM) at time 0. For phototoxicity, experiments started after 10 min blue-light irradiation of cells preloaded with vehicle or sublethal doses of A2E (5 μM) or ATRD (20 μM) 24 h earlier. Cells were monitored at 30-min intervals for NUC405 (blue = caspase 3 activation) or DRAQ7 (red= plasma membrane leakage), respectively. (*C*) A2E (20 μM) lethal toxicity was not prevented by MβCD, while MβCD completely rescued cells from 500 μM Triton X-100 detergent cytotoxicity ($P < 0.001$, mean ± SEM, $n = 3$, two-tailed t test). (*D*) Inhibition of the main effector pathways of programed cell death: disulfiram for Gasdermin-D/pyroptosis; Deferoxamine (DFO) for ferroptosis; and NSA for MLKL/necroptosis ($n = 3$). (*E* and *F*) Dose-dependent phosphorylation and polymerization of MLKL by A2E and ATRD. (*G*) Protection from lipofuscin by Nec7 (mean ± SEM, $P < 0.01$, two-tailed t test, $n = 3$). (*H*) WB showing Nec7 but not Nec1 prevents MLKL phosphorylation/polymerization. (*I*) ARPE-19 monolayers with A2E or ATRD accumulations display phospho-MLKL in plasma membranes which was blocked by Nec7. (Scale bars, 20 μm.)

not (Fig. 4*H*). Furthermore, using confocal fluorescence microscopy, we observed that Ser358 phospho-MLKL localized into membranes in cells with aberrant levels of A2E and ATRD but not in healthy controls (Fig. 4*I*) and that Nec7 treatment effectively prevented the plasma membrane localization of phospho-MLKL. Collectively, our in vitro data suggest that lipofuscin induces an uncharacterized type of necrosome that involves neither RIPK1 nor RIPK3.

Finally, since it has been suggested that apart from the adverse effects of lipid-bisretinoids, the retina of Abca4$^{-/-}$Rdh8$^{-/-}$ succumbs from the toxicity of the ATR released upon illumination (45), we investigated whether ATR could cause necroptosis. Using our cell-death assay, we found that ATR indeed triggered a light-independent cell death in ARPE19 cells (*SI Appendix*, Fig. S4*G*), but the mechanism was no necroptosis as it was insensitive to Nec1 as well as Nec7 (*SI Appendix*, Fig. S4*H*) with no increase in the phosphorylation/polymerization of MLKL (*SI Appendix*, Fig. S4*I*). Overall, these results indicate that necroptosis is a specific consequence of ocular lipofuscin toxicity, distinct from ATR's poisonous effects.

How Lipofuscin Triggers Necroptosis. Because lipofuscin can trigger oxidative stress through light-independent reactions (46), we investigated, using CellROX Deep Red, the generation of reactive oxygen species (ROS) during necroptosis. In the dark, cellular ROS were detectable only in mitochondria

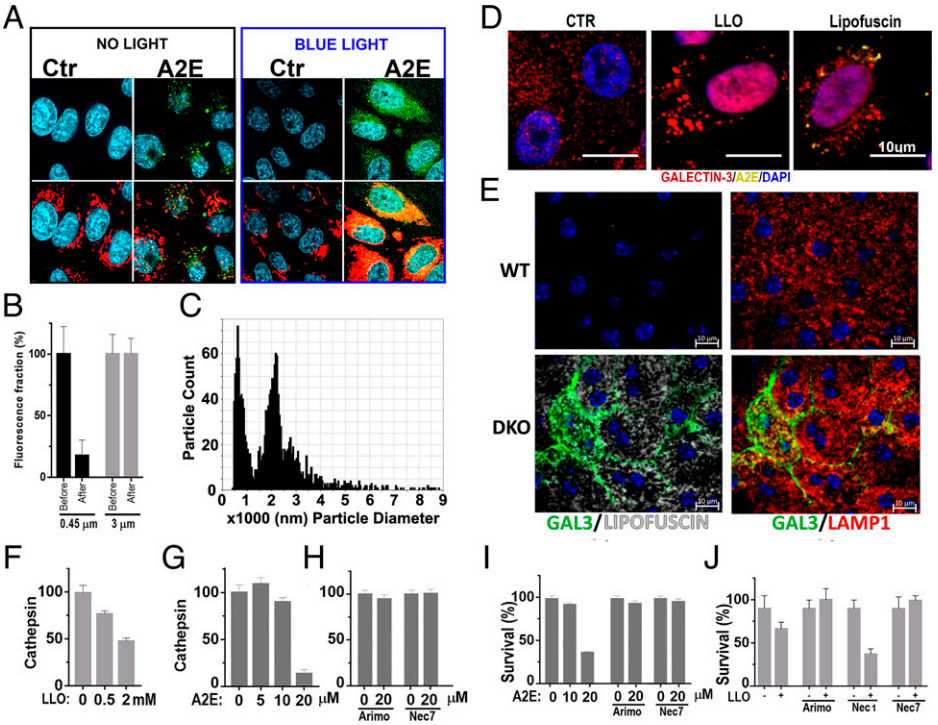

Fig. 5. (*A*) Cellular ROS (red) were detected in mitochondria but not in lipofuscin granules (green). Only after blue-light exposure, ROS colocalized with lipofuscin. (*B*) A2E (MW = 592) passed through 3-µm but not 0.45-µm filters, suggesting that it forms aggregates. (*C*) Particle size measurement using TRPS shows that A2E formed aggregates larger than 500 nm in PBS. (*D*) Galectin-3 puncta assay in ARPE19 to evaluate LMP. Both the positive control LLOMe and A2E induced LMP. (*E*) Increased LMP in DKO retinas with lipofuscin. Galectin-3 puncta positive staining in lysosomes of cells in RPE eyecups from 20-mo-old DKO but not WT mice. (Scale bar, 10 µm.) (*F*) Loss of cathepsins activity in cells exposed to LLOMe doses or (*G*) A2E. (*H*) Loss of cathepsin activity can be prevented with arimoclomol or Nec7 in A2E loaded cells. (*I*) Arimoclomol or Nec7 promote survival to A2E accumulation. (*J*) The LMP inducer LLOMe promotes a necroptosis preventable with Nec7 and arimoclomol but not Nec1.

and not in lipofuscin granules. Yet, when the cells were illuminated with blue light, the granules shattered, and the autofluorescent material spread and became positive for ROS (Fig. 5*A*). Thus, although this method was sensitive to detect lipofuscin-elicited ROS, we found no indication of the occurrence of lipofuscin oxidation during necroptosis. Additionally, we confirmed that antioxidants (NAC, L-cysteine, Vitamin C, TROLOX, BHA, and TMB) did not improve survival against any dose of lipofuscin (*SI Appendix*, Fig. S5).

Since accumulation of crystalline materials in cells can elicit necroptosis (47) and atomic force microscopy revealed that the core of lipofuscin granules comprises solid aggregates (48), we investigated whether lipid-bisretinoids might be forming crystals that kill cells. Thus, we first showed that A2E (MW:592 Da) in aqueous milieu formed large aggregates that could not move across 450-nm filter pores (Fig. 5*B*). This inability to pass was due to size exclusion and not to nonspecific binding, as A2E did cross membranes with 3-µm cutoff of the same material. Next, we exactly determined the size and abundance of A2E aggregates using tunable resistive pulse sensing (TRPS). The basic principle underlying TRPS is that when a particle, suspended in a weakly conducting fluid, flows through a nano constriction electrically sensed, the particle causes a change in the electrical resistance proportional to its size. In this way, we determined that A2E formed large aggregates of around 650 nm and 2,200 nm (Fig. 5*C*).

Next, we investigated whether the suspected A2E crystals were able to damage lysosomal membranes (49). We used the galectin 3 puncta assay for early detection of LMP. Briefly, cytosolic galectin-3 binds to the glycocalyx in the luminal face of lysosomal membranes as they become leaky, which is detectable with anti-galectin, high-affinity antibodies (50). We used L-Leucyl-L-Leucine methyl ester (LLOMe) treatment as LMP-positive control. A2E buildups clearly caused puncta staining and therefore LMP (Fig. 5*D*). Next, we investigated the occurrence of LMP in vivo. Flat-mounted RPE eyecups from 20-mo-old DKO and WT mice were immunostained with anti-galectin3, anti-lamp1, and DAPI. Gal3 puncta was effectively detected in many Lamp1+ RPE's compartments of DKO but not of WT eyes, which coincidently contained detectable levels of lipofuscin (Fig. 5*E*). We further confirmed LMP by showing the inactivation of lysosomal cathepsins (51). Indeed, both LLOMe (Fig. 5*F*) and A2E (Fig. 5*G*) caused reduction in cathepsin activity. Interestingly, loss of cathepsin was prevented by arimoclomol, a drug that promotes lysosomal integrity through the up-regulation of heat shock proteins (52), as well as by Nec7, the only necrostatin that protected against lipofuscin (Fig. 5*H*). Furthermore, we found that arimoclomol protected against necroptosis (Fig. 5*I*), Also, remarkable was the observation that the same unique pattern of protection with arimoclomol and Nec7 but not Nec1 was observable for LLOMe (Fig. 5*J*), consistent with the idea that necroptosis by A2E is being caused by LMP.

Evidence for Lipofuscin-Mediated Necroptosis In Vivo. To study whether pigmented retinas loaded with lipofuscin displayed signs of necroptosis, we evaluated the deposition of phospho-MLKL in flat-mounted RPE eyecups from 2-, 12-, and 27-mo-old DKO and WT C57BL6 mice. Eyecups devoid of neuroretina were immunostained with anti–phospho-Ser358 MLKL. While expression of phospho-MLKL was barely detected in WT retinas, even at 27 mo of age, DKO animals started showing phospho-MLKL staining at 2-mo, which became increasingly positive, first intracellularly, and later at

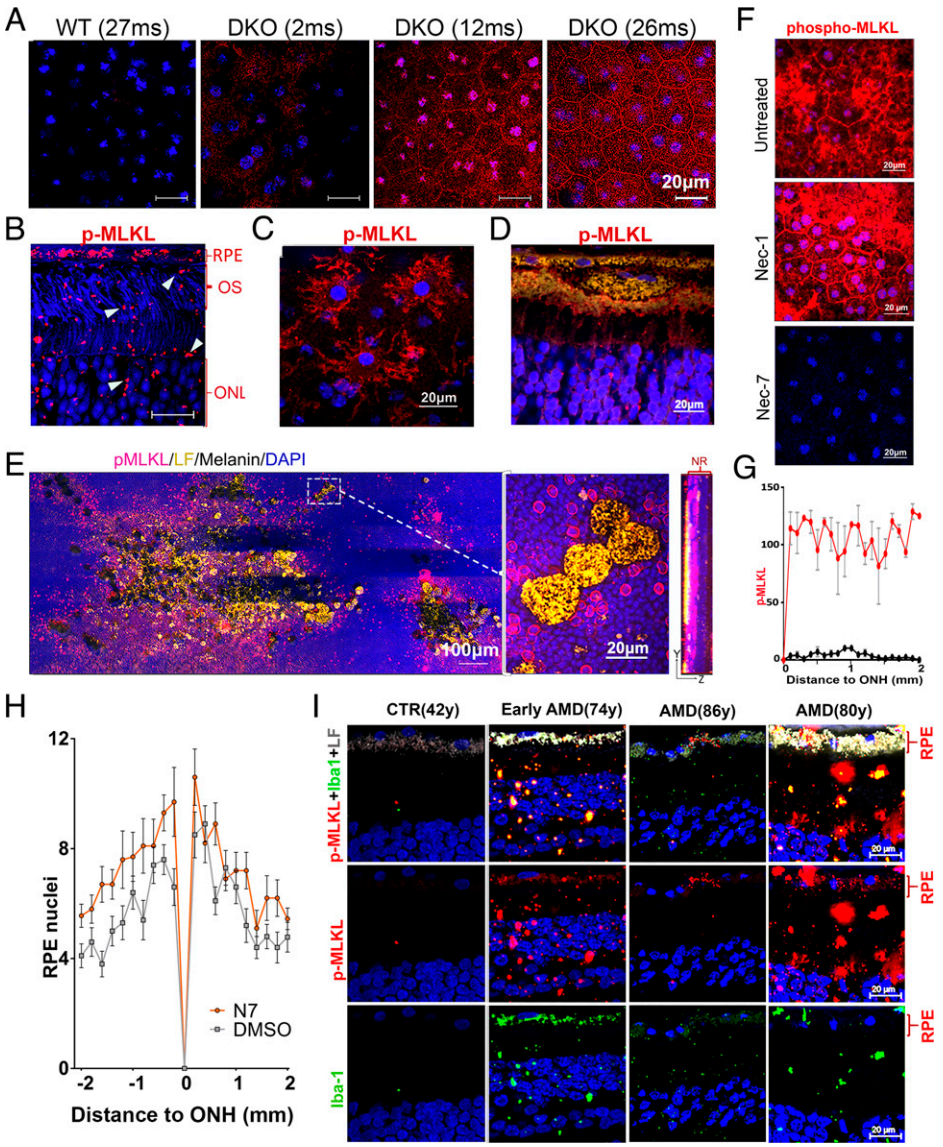

Fig. 6. Necroptosis in retinas with lipofuscin. Central-RPEs, in flat-mounted DKO eyecups immune-stained with (*A*) anti-phospho-Ser345-MLKL (red) and DAPI (blue) ($n = 4$) (Scale bars, 20 μm.) (*B*) ~1 to 3 μm lipofuscin debris (characterized in Fig. 2 as lipofuscin+, iba1+) were positive for phospho-MLKL (red) in demelanized paraffin cross-section from 20-mo-old DKO. (*C*) Microglia/macrophages attached to flat-mounted RPE eyecups from 20-mo-old DKO stained for phospho-MLKL. (*D*) Phospho-MLKL staining (red) of large RPE debris (yellow) shed into neuroretina. (*E*) Stitched panoramic of flat-mounted neuroretina containing clusters of large (~10 μm) RPE fragments, described in Fig. 2 *F* and *H*. Very noticeable was the strong halo of phospho-MLKL (red) around these RPE inclusions. *Right* panel is the maximal projection of one of these lesions, obtained with 63× objective. It shows the spread of the phospho-MLKL signal in the ONL layer in contact with the invading RPE fragments. (*F*) Single intravitreal injection of Nec7 (DKO at 718 d-old, $n = 4$) but not Nec1 (DKO at 709 d-old, $n = 4$) eliminated phospho-MLKL staining in 20-mo-old DKO retinas ($n = 4$). (*G*) Phospho-MLKL expression in RPE flat mounts from 23-mo-old DKO, measured every 0.1-mm interval and plotted as a function of the distance from ONH in inferior hemiretina. Mock- (red line) and Nec7- (black line) treated eyes (**$P < 0.01$ by two-way ANOVA, $n = 3$). (*H*) Intraocular treatment with Nec7 ($n = 10$) prevented loss of RPE nuclei in DKOs compared to mock-treated eyes ($n = 10$) (mean ± SEM, $P = 0.015$, by *t* test, two samples equal variance). (*I*) Human retinas stained with anti-phospho-MLKL (red) and Iba1 (green). The staining was stronger in retinas with abundant lipofuscin and appeared in RPE, Iba1+ cells as well as in debris/fragments infiltrating neuroretina. Donors of 86 y and 80 y had advanced dry AMD diagnosis.

the plasma membrane (Fig. 6*A*). To visualize the distribution of necroptosis markers across the different retinal layers, we stained phospho-MLKL in paraffin cross-sections depleted of melanin from 20-mo-old DKO animals (Fig. 6*B*). The strongest staining for phospho-MLKL was found in cells with abundant lipofuscin content (i.e., RPE layer and small Iba-1+ and CD11b+) (microglia/macrophage). The phospho-MLKL staining was particularly evident for Iba1+ cells infiltrated into the subretinal space of flat mounts from 20-mo-old DKO (Fig. 6*C*). Phospho-MLKL labeling was strong around the large pieces of RPE containing lipofuscin, suggesting the staining originated mainly from microglia/macrophages encapsulating the sloughed RPE fragments (Fig. 6*D*). Very impressive was the discovery of a vast phospho-MLKL staining around the zones of the neuroretina, in which the large RPE fragments had migrated (Fig. 6*E*). This staining could represent that adjacent photoreceptors are undergoing necroptosis or that phospho-MLKL–positive cells, piggy-bagged by the migrated RPE, are dispersing into the area. In either case, the intense phospho-MLKL staining appears to precede and correlate well with the exacerbated loss of photoreceptors in areas bordering the large RPE fragments, as shown in Fig. 2 and *SI Appendix*, Fig. S2*B*.

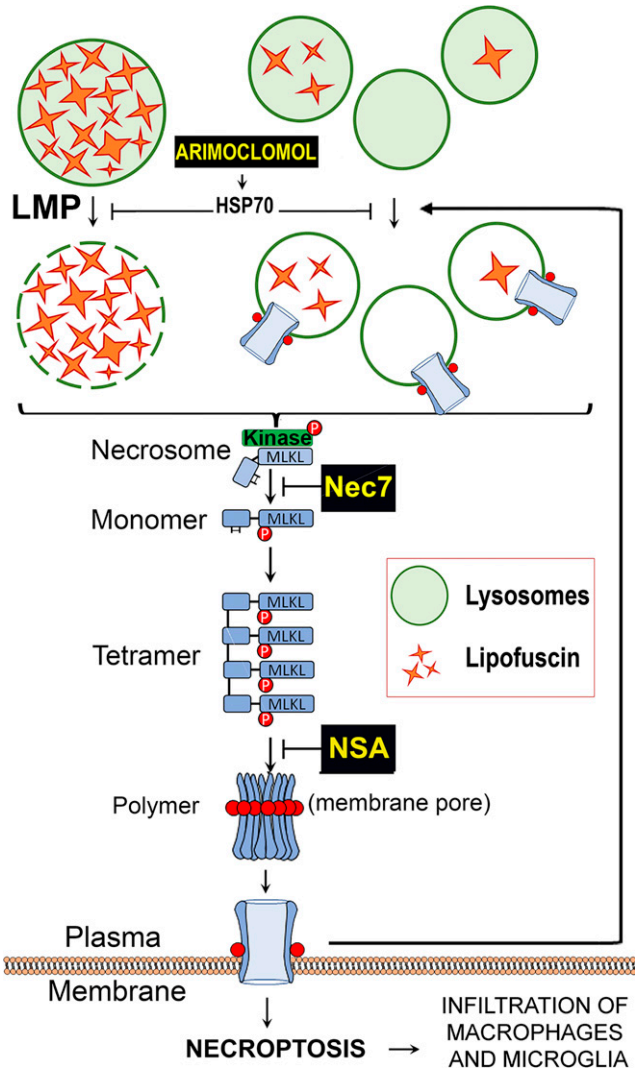

Fig. 7. Working model of light-independent cytotoxicity elicited by the accumulation of lipofuscin. Lipofuscin forms solid crystals that, when in high amounts, damage the lysosomal membranes and cause LMP. The release of lysosomal enzymes triggers the formation of an atypical necrosome that phosphorylates MLKL, promoting its oligomerization and membranes translocation. Phospho-MLKL destabilizes the membrane of lysosomes promoting more LMP. When the levels of phospho-MLKL in plasma membrane become intolerable, the cell undergoes necroptosis.

To establish the therapeutic potential of inhibiting the atypical necroptosis pathway, we injected intraocularly 2 μL of necrostatins, or vehicle, in the eyes of 26-mo-old DKO mice. A week later, we evaluated the status of their retinas by staining RPE and neuroretina flat mounts with anti–phospho-MLKL antibody. We verified that Nec7 but not Nec1 reduced membrane and cytosolic phospho-MLKL staining to undetectable levels (Fig. 6*F*), supporting the notion that the atypical necroptosis pathway detected in our in vitro system was active in retinas loaded with lipofuscin. Fig. 6*G* depicts the phospho-MLKL mean fluorescence expression values of four vehicles and four Nec7 treated eyes, measured every 0.1-mm interval from the optic nerve head (ONH) in RPE flat-mounted inferior hemiretinas from 24-mo-old DKO. The staining became negative from the center to the periphery in Nec7-treated eyes while remained strongly positive in the companion mock-treated eyes. To determine whether inhibition of necroptosis was sufficient to stop the loss of RPE cells, we treated 10 7-mo-old DKOs with 2 μl Nec7 in the right eye and 2 μl vehicle in the left eye every other month for 6 mo, three times in total. At the end of the treatment, the mice were killed, and we counted the number of RPE nuclei. We found that loss of RPE cells was larger in mock-treated eyes than in those that received Nec7 (Fig. 6*H*). In summary, the results show that blockage of necroptosis with Nec7 significantly reduces the signs of RPE degeneration.

To analyze the impact of treatment on photoreceptors, we compared phospho-MLKL expression in neuroretina flat mounts from control and Nec7-treated eyes. We observed that the necroptosis labeling was significantly reduced by Nec7 (*SI Appendix*, Fig. S6*A*). Similarly, Nec7 reduced the infiltration of CD11b cells in the subretinal space, as shown by the disappearing of Iba1+ cells on RPE flat mounts from 18- to 20-mo-old DKO mice (*SI Appendix*, Fig. S6*B*).

To investigate the relevance of lipofuscin-induced necroptosis cascade in humans, we performed immunofluorescence staining of phospho-MLKL and Iba1 in retinal cryo-sections. Slides containing control and dry AMD human retina sections from the midperiphery, in proximity to the macula, showed phospho-MLKL expression in the RPE as well as in Iba1+ infiltrates. The intensity and frequency of positive structures correlated well with the amount of lipofuscin accumulated. In one 86-y-old eye with advanced nonneovascular AMD diagnosis, the RPE content of lipofuscin was low and phospho-MLKL pattern was restricted to small zones in the RPE (Fig. 6*I*).

Based on our observations, we generated a model that summarizes these data and explains the mechanism underlaying light-independent lipofuscin cytotoxicity (Fig. 7). According to this working model, lipofuscin accumulation causes mild-LMP that elicits the assembly of an atypical necrosome, which in turn mediates MLKL phosphorylation/polymerization. Phospho-MLKL oligomeric structures progressively insert into cellular membranes of lysosomes and plasma membrane, causing more LMP, which in turn promotes more phospho-MLKL deposition on cell membranes. This creates a vicious loop until the number of phospho-MLKL pores per cell is such that the cell undergoes a necroptotic break down.

Discussion

All ongoing clinical trials to treat lipofuscin-associated pathologies are testing drugs that reduce the formation of lipofuscin, making them good candidates to prevent rather than to remediate degenerations in retinas with established deposits (53). New strategies that could help deal with lipofuscin buildups include the use of removal agents (54) or the approach investigated here (i.e., inhibitors of toxic cascades originating from the granules). The current view is that in the retina, lipofuscin's toxic cascades originate mainly from the photooxidation of its lipid-bisretinoid constituents, which trigger apoptosis (55). Although this "phototoxicity cell death" hypothesis has been around for many years (20, 21), there is still not evidence that antiapoptotic agents or blue-light blocking lenses stop degenerations by lipofuscin (56, 57). Antioxidant therapy have shown no effect to prevent the onset of AMD (58). The Age-Related Eye Disease Studies (AREDS) 1 and 2 trials showed that prolonged megadose consumption of antioxidants and minerals may reduce the risk of progression of AMD in some individuals with intermediate/advanced disease (59); however, the authors of the trials could not issue a blanket recommendation for the use of AREDS supplements for AMD (60). In addition, there is no indication that AREDS supplements are of any benefit for Stargardt patients. These suggest the urgent need to revise the pathogenesis of lipofuscin granules in order to develop more effective therapies. Protection against phototoxicity may need

to be combined with other approaches in order to benefit Stargardt and all AMD patients.

Here, we provide evidence that lipofuscin has the tendency to form solid aggregates that cause LMP, which in turn trigger atypical necrosomes that cause more LMP through membrane translocation of phospho-MLKL oligomeric pores, perpetuating a harmful cycle that culminates with the necrotic release of the inflammatory content of cells loaded with lipofuscin. The lethal cascade is controllable with a completely different set of pharmacological inhibitors from those used to ameliorate photooxidative stress.

Phospho-MLKL oligomerization was detectable in vitro, in the retinas of the DKO model with still low to medium levels of lipofuscin, and in individuals with early and late dry AMD (Figs. 4 and 6). The age-related increase of lipofuscin in Abca4$^{-/-}$Rdh8$^{-/-}$ animals correlated with the number of granules observed per RPE cell (Fig. 1) and previous studies using quantitative fundus autofluorescence (61). Lipofuscin increase was accompanied by a reduction in the number and enlargement in the size of RPE cells, which probably reflects the expansion of surviving cells to seal the gaps created by the death or shedding of cell fragments loaded with lipofuscin. In agreement with a previous report (62), we noticed the infiltration of the outer retina with Iba1+/CD11b+ cells, which likely amplified the local inflammation and cell death (Fig. 2 and *SI Appendix*, Fig. S2). Furthermore, we noticed the appearance of small photoreceptors (1 to 3 μm) and large RPE (5 to 10 μm) fragments that could represent the equivalents to flecks (63) or sloughed cells (64) in Stargardt and dry AMD retinas, respectively. These debris may also be originated by the increased phospho-MLKL activity that promotes secretion as a way to reduce necroptosis (26). We also noticed debris in human retinas with phospho-MLKL staining. Further investigations will be needed to decide the origin and significance of these debris.

The comparable loss of photoreceptors and RPE cells between dark- and light-reared DKO (Fig. 3) shows that light-independent toxicity of the granules plays a major role in the degeneration in vivo. The photobleaching of DKO retinas under cyclic light indicates that there is some photooxidation of the lipofuscin in pigmented animals (*SI Appendix*, Fig. S3).

Lipofuscin affected the RPE more in the inferior hemisphere than in the superior one (Fig. 3). Similar upper/lower degenerative asymmetry in retinas of DKOs has been reported before (27) and cannot be attributed to photodamage because 1) the degeneration was undeterred in our dark-reared DKOs, and 2) the photobleaching of the lipofuscin occurred evenly in both hemispheres (*SI Appendix*, Fig. S3). Considering that we found no evidence of more autofluorescence in the inferior hemispheres, it is possible that the RPE in the inferior part is more vulnerable to lipofuscin. Superior versus inferior retinal gene expression differences have been previously reported and may account for this distinct susceptibility (65, 66).

A landmark finding in this study was the discovery that light-independent lipofuscin cytotoxicity elicited an atypical form of necroptosis, rather than apoptosis, previously associated with blue-light phototoxicity (21, 22). The evidence for light-independent, lipofuscin-mediated necroptosis was strong and multifaceted (Fig. 4): 1) real-time monitoring of cell death showed early compromise in membrane integrity without caspase 3 activation; 2) lipofuscin induced a dose-dependent Ser358 phosphorylation, polymerization, and plasma membrane translocation of MLKL in light-free conditions; 3) cell death was preventable with NSA; 4) RPE cell death in the dark could not be prevented by the pan-caspase inhibitor z-VAD(OMe)-FMK or antioxidants; and 5) Nec7 prevented MLKL phosphorylation, polymerization, plasma membrane localization, and cell death by lipofuscin. Necroptosis has been previously described in the context of hypoxia caused by retinal detachment (67) and ROS, using both in vitro and in vivo agents like hydrogen peroxide, tert-butyl hydroperoxide, and sodium iodate to induce geographic atrophy (68). Both hypoxic- and ROS-triggered necroptosis relied on the core RIPK1–RIPK3–MLKL necrosome for execution and accordingly were blocked with antioxidants as well as genetic or chemical inhibitors of RIPK1 and RIPK3 (69, 70). In striking contrast, lipofuscin-elicited cell death and MLKL phosphorylation/polymerization was neither affected by RIP1 kinase inhibitors Nec1, Nec1s, Nec2, and Nec5 nor by treatment with RIPK3 inhibitors (Fig. 4*G*) or antioxidants (*SI Appendix*, Fig. S5*A*). Taken together, these findings support the notion that lipofuscin promotes the formation of an undescribed necrosome that does not contain RIPK1 nor RIPK3. Accordingly, previous studies of necroptosis in the retina are not relevant to identify pharmacological targets against lipofuscin-driven RPE cell death. Further genetic and chemical knockdown experiments are in progress to understand the necrosome composition induced during lipofuscin accumulation. We propose that chronic accumulation of polymeric phospho-MLKL pores contribute to the progressive failure of RPE in retinas with increasing lipofuscin buildup. Cell membrane disruption by phospho-MLKL oligomers not only predicts the atrophic changes in the RPE layer but the release of cellular constituents that are known to elicit local inflammation (71). Thus, our findings could have important additional implications for the pathobiology of retinal atrophy and could explain the recruitment of activated microglia/macrophages we observed here.

Crystal accumulation plays a defining role in the pathogenesis of a range of common diseases such as lysosomal storage disorders and atherosclerosis (72, 73). Many studies have now elucidated a connection between insoluble crystalline deposits and necroptosis (74, 75). Pertinently, we confirmed LMP in cells with lipofuscin both in vitro (Fig. 5) and in vivo (*SI Appendix*, Fig. S6). Loss of cathepsins' activity without evident release of the enzymes into the cytosol, or extracellular media, was a very reproducible and characteristic feature of cells with A2E. The same cellular defect was reported by Repnik et al. (51) in cells exposed to low doses of LLOMe, a peptide that induces LMP. Moderate LMP caused reversible lysosomal membrane damage that allowed the escape of small molecules (<10 kDa) and ions but not cathepsins, which became inactivated while still trapped. Our results are supported by published data (76) that shows differentiated ARPE-19 cultures loaded with A2E exhibit compromised cathepsin D and acid lysosomal phosphatase activities. In the same direction, electron microscopy images of DKO retinas provide evidence for increased disturbed lysosomal membrane integrity with age (77). Furthermore, we confirmed the occurrence of LMP in lipofuscin-occupied cells using other independent methods: the galectin-3 puncta assay and the protection with arimoclomol on both cathepsin activity and cell viability (Figs. 5 and 6). Because moderate LMP does not release cathepsins into the cytosol, it cannot trigger the typical proteolytic signaling cascade that leads to apoptosis, but instead, it provokes the restauration of the activity of the hydrolases (51), possibly through lysosomal stress and biogenesis.

Pertinently, the expression of phospho-MLKL became stronger, and the association with plasma membrane became clearer, both in vitro and in the DKO retinas, as cells became more overloaded with lipofuscin (Fig. 6). Intraocular treatment with Nec7 but not Nec1 ablated the necroptosis label (Fig. 6) and prevented the preferential loss of RPE cells in the inferior hemisphere (Fig. 6*H*), indicating that 1) the antibody staining was specific, 2) the atypical necroptosis loop occurred in the retina, validating the relevance of the pathway identified in vitro, and 3) atypical necroptosis mediated by lipid-bisretinoids was a main driver of retinal damage. Not only RPE but also CD11b+ and Iba1+ infiltrates were positive for phospho-MLKL, as they were also loaded with lipofuscin. Analysis of human samples revealed a pattern of phospho-MLKL positivity on Iba1+ and RPE cells very similar to the

one found in old DKO retinas. The 86-y-old retina with dry AMD and low lipofuscin that displayed few localized phospho-MLKL patches in the RPE layer may represent the late stage of the atrophic disease when most cells are already gone (Fig. 6*I*). Collectively, our data underscore the potential importance of phospho-MLKL oligomerization and subsequent execution of necroptosis in retinal cells containing lipofuscin (Fig. 7). Although several mechanistic details of this choreography remain to be revealed, the demonstration that lipofuscin granules elicit deleterious LMP necroptosis may have therapeutic importance, since each checkpoint in this pathway could represent a possible target for pharmacologic intervention or a marker for degeneration and disease progression.

Materials and Methods

Cells. ARPE-19 (ATCC CRL-2302) and hfRPE cells were cultured in Dulbecco's Modified Eagle Medium 10% fetal bovine serum and 1% penicillin/streptomycin. hfRPE were grown following published protocol (78).

In Vivo Treatment. For short-term treatments, 2 μL of 33 mM Nec7 in dimethyl sulfoxide (DMSO) were intravitreally injected in the left eye, and an equal amount of vehicle (DMSO) was administered to the right eye.

Animals were killed 1 wk later and phospho-MLKL levels assessed in the retinas.

For long-term treatments, 10 7-mo-old DKOs and WT received 2 μl Nec7 in the right eye and 2 μl vehicle in the left eye every other month for 6 mo, three times in total.

Lipofuscin/Cell. A2E-loaded ARPE19 cells were trypsinized, counted, and resuspended in lysis buffer (2% Triton X-100) for fluorescence quantification. For eye's RPE, 12-mo-old WT and DKO mice were killed, RPE separated from neuroretina by dissection and from an underlying choroid by incubating 10 min eyecups in 100 uL of RNA Protect Reagent from Qiagen (Catalog no. 76526) as described (79). Mouse RPE were counted and lysed in 2% Triton X-100. Fluorescence of the lysates (arbitrary units) was measured with a Spectramax M5s (430-nm excitation/600-nm emission).

Lipofuscin Aggregation. Fluorescence (Ex 435 nm/Em 600 nm) of 500 μM A2E or ATRD solutions in phosphate buffered saline (PBS) were measured before and after filtration through 0.45-μm or 3-μm nylon syringe filters (Tisch Scientific). TRPS method (Izon Sciences, Boston) was used for exactly determined size of A2E aggregates. Briefly, 45 μL A2E in PBS (500 μM) were pipetted into nanopore membranes (NP150, NP300, NP600, NP800, and NP4000), and then double-pressure recording and voltage were applied. Every single particle caused a resistive pulse that was used to calculate particle size and concentration. Polystyrene nanoparticles of different known sizes and concentrations were used for calibration.

Data Availability. All study data are included in the article and/or *SI Appendix*.

ACKNOWLEDGMENTS. Funding was provided by the following grants: BrightFocus-M2016124 to M.M.N.; National Eye Institute, R01EY027422 to M.M.N.; and R01EY08538 and GM34107 to E.R.-B. Research to Prevent Blindness grants to the Departments of Ophthalmology at Weill Cornell Medicine (WCM) and University of California, Los Angeles, Stein Eye Institute. Thanks to Sheldon Miller and Maminishkis for providing hfRPE; Sushmita Mukherjee at WCM for setup ONL-thickness analysis; Vera Bonilha, Cleveland Clinic for invaluable help with human specimens; and Zelda Salfati for maintaining the colony.

1. K.-P. Ng *et al.*, Retinal pigment epithelium lipofuscin proteomics. *Mol. Cell. Proteomics* **7**, 1397–1405 (2008).
2. R. Gómez-Sintes, M. D. Ledesma, P. Boya, Lysosomal cell death mechanisms in aging. *Ageing Res. Rev.* **32**, 150–168 (2016).
3. K. Ono, S. O. Kim, J. Han, Susceptibility of lysosomes to rupture is a determinant for plasma membrane disruption in tumor necrosis factor alpha-induced cell death. *Mol. Cell. Biol.* **23**, 665–676 (2003).
4. U. Brunk, A. Brun, The effect of aging on lysosomal permeability in nerve cells of the central nervous system. An enzyme histochemical study in rat. *Histochemie* **30**, 315–324 (1972).
5. J. R. Sparrow, B. Cai, Y. P. Jang, J. Zhou, K. Nakanishi, *A2E, a Fluorophore of RPE Lipofuscin, Can Destabilize Membrane* in Advances in Experimental Medicine and Biology, 2005, pp. 63–68.
6. O. A. Anderson, A. Finkelstein, D. T. Shima, A2E induces IL-1ß production in retinal pigment epithelial cells via the NLRP3 inflammasome. *PLoS One* **8**, e67263 (2013).
7. M. A. Katsnelson, K. M. Lozada-Soto, H. M. Russo, B. A. Miller, G. R. Dubyak, NLRP3 inflammasome signaling is activated by low-level lysosome disruption but inhibited by extensive lysosome disruption: Roles for K+ efflux and Ca2+ influx. *Am. J. Physiol. Cell Physiol.* **311**, C83–C100 (2016).
8. L. Feeney-Burns, E. S. Hilderbrand, S. Eldridge, Aging human RPE: Morphometric analysis of macular, equatorial, and peripheral cells. *Invest. Ophthalmol. Vis. Sci.* **25**, 195–200 (1984).
9. G. E. Eldred, M. R. Lasky, Retinal age pigments generated by self-assembling lysosomotropic detergents. *Nature* **361**, 724–726 (1993).
10. A. Moreno-García, A. Kun, O. Calero, M. Medina, M. Calero, An overview of the role of lipofuscin in age-related neurodegeneration. *Front. Neurosci.* **12**, 464 (2018).
11. A. Terman, Garbage catastrophe theory of aging: Imperfect removal of oxidative damage? *Redox Rep.* **6**, 15–26 (2001).
12. R. W. Young, D. Bok, Participation of the retinal pigment epithelium in the rod outer segment renewal process. *J. Cell Biol.* **42**, 392–403 (1969).
13. F. Mazzoni, H. Safa, S. C. Finnemann, Understanding photoreceptor outer segment phagocytosis: Use and utility of RPE cells in culture. *Exp. Eye Res.* **126**, 51–60 (2014).
14. H. J. Kim, J. R. Sparrow, Bisretinoid phospholipid and vitamin A aldehyde: shining a light. *J. Lipid Res.* **62**, 100042 (2021).
15. F. Quazi, R. S. Molday, ATP-binding cassette transporter ABCA4 and chemical isomerization protect photoreceptor cells from the toxic accumulation of excess 11-cis-retinal. *Proc. Natl. Acad. Sci. U.S.A.* **111**, 5024–5029 (2014).
16. T. L. Lenis *et al.*, Expression of ABCA4 in the retinal pigment epithelium and its implications for Stargardt macular degeneration. *Proc. Natl. Acad. Sci. U.S.A.* **115**, E11120–E11127 (2018).
17. T. R. Burke *et al.*, Quantitative fundus autofluorescence in recessive Stargardt disease. *Invest. Ophthalmol. Vis. Sci.* **55**, 2841–2852 (2014).
18. A. E. Sears *et al.*, Towards treatment of stargardt disease: Workshop organized and sponsored by the foundation fighting blindness. *Transl. Vis. Sci. Technol.* **6**, 6 (2017).
19. J. R. Sparrow, Vitamin A-aldehyde adducts: AMD risk and targeted therapeutics. *Proc. Natl. Acad. Sci. U.S.A.* **113**, 4564–4569 (2016).
20. M. Boulton, A. Dontsov, J. Jarvis-Evans, M. Ostrovsky, D. Svistunenko, Lipofuscin is a photoinducible free radical generator. *J. Photochem. Photobiol. B* **19**, 201–204 (1993).
21. J. R. Sparrow, K. Nakanishi, C. A. Parish, The lipofuscin fluorophore A2E mediates blue light-induced damage to retinal pigmented epithelial cells. *Invest. Ophthalmol. Vis. Sci.* **41**, 1981–1989 (2000).
22. J. R. Sparrow, B. Cai, Blue light-induced apoptosis of A2E-containing RPE: Involvement of caspase-3 and protection by Bcl-2. *Invest. Ophthalmol. Vis. Sci.* **42**, 1356–1362 (2001).
23. K. Ueda, J. Zhao, H. J. Kim, J. R. Sparrow, Photodegradation of retinal bisretinoids in mouse models and implications for macular degeneration. *Proc. Natl. Acad. Sci. U.S.A.* **113**, 6904–6909 (2016).
24. G. Karan *et al.*, Lipofuscin accumulation, abnormal electrophysiology, and photoreceptor degeneration in mutant ELOVL4 transgenic mice: A model for macular degeneration. *Proc. Natl. Acad. Sci. U.S.A.* **102**, 4164–4169 (2005).
25. E. Flynn, K. Ueda, E. Auran, J. M. Sullivan, J. R. Sparrow, Fundus autofluorescence and photoreceptor cell rosettes in mouse models. *Invest. Ophthalmol. Vis. Sci.* **55**, 5643–5652 (2014).
26. S. Yoon, A. Kovalenko, K. Bogdanov, D. Wallach, MLKL, the protein that mediates necroptosis, also regulates endosomal trafficking and extracellular vesicle generation. *Immunity* **47**, 51–65.e7 (2017).
27. A. Maeda, T. Maeda, M. Golczak, K. Palczewski, Retinopathy in mice induced by disrupted all-trans-retinal clearance. *J. Biol. Chem.* **283**, 26684–26693 (2008).
28. N. P. Boyer *et al.*, Lipofuscin and N-retinylidene-N-retinylethanolamine (A2E) accumulate in retinal pigment epithelium in absence of light exposure: Their origin is 11-cis-retinal. *J. Biol. Chem.* **287**, 22276–22286 (2012).
29. J. R. Sparrow, S. R. Kim, Y. Wu, "Experimental approaches to the study of A2E, a bisretinoid lipofuscin chromophore of retinal pigment epithelium" in *Methods in Molecular Biology*, H. Sun, G. H. Travis, Eds. (Humana Press, Totowa, NJ, 2010), pp. 315–327.
30. A. Maeda *et al.*, Primary amines protect against retinal degeneration in mouse models of retinopathies. *Nat. Chem. Biol.* **8**, 170–178 (2011).
31. A. R. Wielgus, C. F. Chignell, P. Ceger, J. E. Roberts, Comparison of A2E cytotoxicity and phototoxicity with all- *trans* -retinal in human retinal pigment epithelial cells. *Photochem. Photobiol.* **86**, 781–791 (2010).
32. S. De, T. P. Sakmar, Interaction of A2E with model membranes. Implications to the pathogenesis of age-related macular degeneration. *J. Gen. Physiol.* **120**, 147–157 (2002).
33. R. Zidovetzki, I. Levitan, Use of cyclodextrins to manipulate plasma membrane cholesterol content: Evidence, misconceptions and control strategies. *Biochim. Biophys. Acta* **1768**, 1311–1324 (2007).
34. W. J. Degrip, J. Vanoostrum, P. H. Bovee-Geurts, Selective detergent-extraction from mixed detergent/lipid/protein micelles, using cyclodextrin inclusion compounds: A novel generic approach for the preparation of proteoliposomes. *Biochem. J.* **330**, 667–674 (1998).
35. E. Sahin *et al.*, Telomere dysfunction induces metabolic and mitochondrial compromise. *Nature* **470**, 359–365 (2011).
36. D. Wallach, T. B. Kang, C. P. Dillon, D. R. Green, Programmed necrosis in inflammation: Toward identification of the effector molecules. *Science (80-.)* **352**, aaf2154 (2016).

37. Y. Tong, S. Wang, Not all stressors are equal: Mechanism of stressors on RPE cell degeneration. *Front. Cell Dev. Biol.* **8**, 591067 (2020).
38. J. J. Hu *et al.*, FDA-approved disulfiram inhibits pyroptosis by blocking gasdermin D pore formation. *Nat. Immunol.* **21**, 736–745 (2020).
39. S. Ma, E. S. Henson, Y. Chen, S. B. Gibson, Ferroptosis is induced following siramesine and lapatinib treatment of breast cancer cells. *Cell Death Dis.* **7**, e2307 (2016).
40. L. Sun *et al.*, Mixed lineage kinase domain-like protein mediates necrosis signaling downstream of RIP3 kinase. *Cell* **148**, 213–227 (2012).
41. H. Wang *et al.*, Mixed lineage kinase domain-like protein MLKL causes necrotic membrane disruption upon phosphorylation by RIP3. *Mol. Cell* **54**, 133–146 (2014).
42. A. Degterev *et al.*, Identification of RIP1 kinase as a specific cellular target of necrostatins. *Nat. Chem. Biol.* **4**, 313–321 (2008).
43. J. Zhang, Y. Yang, W. He, L. Sun, Necrosome core machinery: MLKL. *Cell. Mol. Life Sci.* **73**, 2153–2163 (2016).
44. W. Zheng, A. Degterev, E. Hsu, J. Yuan, C. Yuan, Structure-activity relationship study of a novel necroptosis inhibitor, necrostatin-7. *Bioorg. Med. Chem. Lett.* **18**, 4932–4935 (2008).
45. A. Maeda *et al.*, Involvement of all-trans-retinal in acute light-induced retinopathy of mice. *J. Biol. Chem.* **284**, 15173–15183 (2009).
46. K. Ueda *et al.*, Iron promotes oxidative cell death caused by bisretinoids of retina. *Proc. Natl. Acad. Sci. U.S.A.* **115**, 4963–4968 (2018).
47. S. R. Mulay *et al.*, Cytotoxicity of crystals involves RIPK3-MLKL-mediated necroptosis. *Nat. Commun.* **7**, 10274 (2016).
48. N. M. Haralampus-Grynaviski *et al.*, Spectroscopic and morphological studies of human retinal lipofuscin granules. *Proc. Natl. Acad. Sci. U.S.A.* **100**, 3179–3184 (2003).
49. F. Wang, R. Gómez-Sintes, P. Boya, Lysosomal membrane permeabilization and cell death. *Traffic* **19**, 918–931 (2018).
50. S. Aits *et al.*, Sensitive detection of lysosomal membrane permeabilization by lysosomal galectin puncta assay. *Autophagy* **11**, 1408–1424 (2015).
51. U. Repnik *et al.*, L-leucyl-L-leucine methyl ester does not release cysteine cathepsins to the cytosol but inactivates them in transiently permeabilized lysosomes. *J. Cell Sci.* **130**, 3124–3140 (2017).
52. T. Kirkegaard *et al.*, Hsp70 stabilizes lysosomes and reverts Niemann-Pick disease-associated lysosomal pathology. *Nature* **463**, 549–553 (2010).
53. M. Gliem *et al.*, Quantitative fundus autofluorescence in early and intermediate age-related macular degeneration. *JAMA Ophthalmol.* **134**, 817–824 (2016).
54. M. M. Nociari, S. Kiss, E. Rodriguez-Boulan, "Lipofuscin accumulation into and clearance from retinal pigment epithelium lysosomes: Physiopathology and emerging therapeutics" in *Lysosomes - Associated Diseases and Methods to Study Their Function*, P. D. Sharma, Ed. (InTech, 2017).
55. J. Zhao, K. Ueda, M. Riera, H. J. Kim, J. R. Sparrow, Bisretinoids mediate light sensitivity resulting in photoreceptor cell degeneration in mice lacking the receptor tyrosine kinase Mer. *J. Biol. Chem.* **293**, 19400–19410 (2018).
56. L. E. Downie, L. Busija, P. R. Keller, Blue-light filtering intraocular lenses (IOLs) for protecting macular health. *Cochrane Database Syst. Rev.* **5**, CD011977 (2018).
57. M. A. Mainster, P. L. Turner, Blue light's benefits vs blue-blocking intraocular lens chromophores. *Graefes Arch. Clin. Exp. Ophthalmol.* **250**, 1245–1246, author reply 1247–1248 (2012).
58. J. R. Evans, J. G. Lawrenson, Antioxidant vitamin and mineral supplements for preventing age-related macular degeneration. *Cochrane Database Syst. Rev.* (7):CD000254 (2012).
59. J. R. Evans, J. G. Lawrenson, Antioxidant vitamin and mineral supplements for slowing the progression of age-related macular degeneration. *Cochrane Database Syst. Rev.* **7**, CD000254 (2017).
60. J. Ambati, B. K. Ambati, Age-related eye disease study caveats. *Arch. Ophthalmol. (Chicago, Ill. 1960)* **120**, 997; author reply 997-9 (2002).
61. J. R. Sparrow *et al.*, Quantitative fundus autofluorescence in mice: Correlation with HPLC quantitation of RPE lipofuscin and measurement of retina outer nuclear layer thickness. *Invest. Ophthalmol. Vis. Sci.* **54**, 2812–2820 (2013).
62. W. Ma, S. Coon, L. Zhao, R. N. Fariss, W. T. Wong, A2E accumulation influences retinal microglial activation and complement regulation. *Neurobiol. Aging* **34**, 943–960 (2013).
63. Y. Solberg *et al.*, Retinal Flecks in Stargardt Disease Reveal Characteristic Fluorescence Lifetime Transition Over Time. *Retina* **39**, 879–888 (2019).
64. T. Ach, *et al.*, Lipofuscin Redistribution and Loss Accompanied by Cytoskeletal Stress in Retinal Pigment Epithelium of Eyes With Age-Related Macular Degeneration. *Invest Ophthalmol Vis. Sci.* **56**, 3242–3252 (2015).
65. T. Maeda *et al.*, Loss of cone photoreceptors caused by chromophore depletion is partially prevented by the artificial chromophore pro-drug, 9-cis-retinyl acetate. *Hum. Mol. Genet.* **18**, 2277–2287 (2009).
66. D. Schulte, T. Furukawa, M. A. Peters, C. A. Kozak, C. L. Cepko, Misexpression of the Emx-related homeobox genes cVax and mVax2 ventralizes the retina and perturbs the retinotectal map. *Neuron* **24**, 541–553 (1999).
67. K. Dong *et al.*, Necrostatin-1 protects photoreceptors from cell death and improves functional outcome after experimental retinal detachment. *Am. J. Pathol.* **181**, 1634–1641 (2012).
68. G. Chowers *et al.*, Course of sodium iodate–induced retinal degeneration in albino and pigmented mice. *Invest. Ophthalmol. Vis. Sci.* **58**, 2239–2249 (2017).
69. J. Hanus *et al.*, Induction of necrotic cell death by oxidative stress in retinal pigment epithelial cells. *Cell Death Dis.* **4**, e965 (2013).
70. J. Hanus, C. Anderson, D. Sarraf, J. Ma, S. Wang, Retinal pigment epithelial cell necroptosis in response to sodium iodate. *Cell Death Discov.* **2**, 16054 (2016).
71. A. Kaczmarek, P. Vandenabeele, D. V. Krysko, Necroptosis: The release of damage-associated molecular patterns and its physiological relevance. *Immunity* **38**, 209–223 (2013).
72. P. Duewell *et al.*, NLRP3 inflammasomes are required for atherogenesis and activated by cholesterol crystals. *Nature* **464**, 1357–1361 (2010).
73. A. Serrano-Puebla, P. Boya, Lysosomal membrane permeabilization in cell death: New evidence and implications for health and disease. *Ann. N. Y. Acad. Sci.* **1371**, 30–44 (2015).
74. A. Alu *et al.*, The role of lysosome in regulated necrosis. *Acta Pharm. Sin. B* **10**, 1880–1903 (2020).
75. X. Y. Sun, J. M. Ouyang, New view in cell death mode: Effect of crystal size in renal epithelial cells. *Cell Death Dis.* **6**, e2013 (2015).
76. E. Poliakov *et al.*, Multiple A2E treatments lead to melanization of rod outer segment-challenged ARPE-19 cells. *Mol. Vis.* **20**, 285–300 (2014).
77. T. Taubitz *et al.*, Ultrastructural alterations in the retinal pigment epithelium and photoreceptors of a Stargardt patient and three Stargardt mouse models: Indication for the central role of RPE melanin in oxidative stress. *PeerJ* **6**, e5215 (2018).
78. A. Maminishkis *et al.*, Confluent monolayers of cultured human fetal retinal pigment epithelium exhibit morphology and physiology of native tissue. *Invest. Ophthalmol. Vis. Sci.* **47**, 3612–3624 (2006).
79. C. Xin-Zhao Wang, K. Zhang, B. Aredo, H. Lu, R. L. Ufret-Vincenty, Novel method for the rapid isolation of RPE cells specifically for RNA extraction and analysis. *Exp. Eye Res.* **102**, 1–9 (2012).